Efficiency Enhancement of PbS Quantum Dot/ZnO Nanowire Bulk-Heterojunction Solar Cells by Plasmonic Silver Nanocubes

Tokuhisa Kawawaki,[†] Haibin Wang,[‡] Takaya Kubo,[‡] Koichiro Saito,[†] Jotaro Nakazaki,[‡] Hiroshi Segawa,[*,‡] and Tetsu Tatsuma[*,†]

[†]Institute of Industrial Science, The University of Tokyo, 4-6-1 Komaba, Meguro-ku, Tokyo 153-8505, Japan and [‡]Research Center for Advanced Science and Technology, The University of Tokyo, 4-6-1 Komaba, Meguro-ku, Tokyo 153-8904, Japan

ABSTRACT

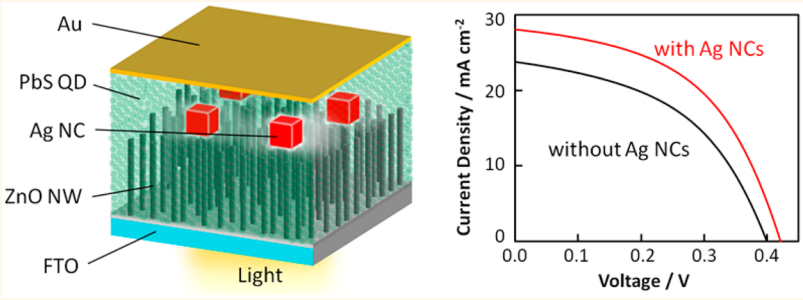

For improvement of solar cell performance, it is important to make efficient use of near-infrared light, which accounts for ~40% of sunlight energy. Here we introduce plasmonic Ag nanocubes (NCs) to colloidal PbS quantum dot/ZnO nanowire (PbS QD/ZnO NW) bulk-heterojunction solar cells, which are characterized by high photocurrents, for further improvement in the photocurrent and power conversion efficiency (PCE) in the visible and near-infrared regions. The Ag NCs exhibit strong far field scattering and intense optical near field in the wavelength region where light absorption of PbS QDs is relatively weak. Photocurrents of the solar cells are enhanced by the Ag NCs particularly in the range 700−1200 nm because of plasmonic enhancement of light absorption and possible facilitation of exciton dissociation. As a result of the optimization of the position and amount of Ag NCs, the PCE of PbS QD/ZnO NW bulk-heterojunction solar cells is improved from 4.45% to 6.03% by 1.36 times.

KEYWORDS: colloidal quantum dot · bulk-heterojunction solar cell · localized surface plasmon resonance · silver nanocube

Efficient harvesting of near-infrared light is of significance for effective use of solar energy. The use of colloidal PbS quantum dots (QDs) is a promising solution[1] because of the tunable, size-dependent band gap from ~0.7 to 1.3 eV.[2] Solution processing is an additional advantage of colloidal QD solar cells. Among the QD solar cells, those with a planar junction between wide band gap n-type semiconductors such as ZnO and p-type PbS QDs have achieved high efficiencies.[3−5] However, their photocurrent in the near-infrared region is still low; external quantum efficiency (EQE) is typically less than 10% at 1100 nm.[3] A bulk-heterojunction structure improves the EQE in both the visible (>80%) and near-infrared (~40% at 1100 nm) regions because of the thick QD layer.[6,7] However, a further increase in the QD layer thickness would increase the internal series resistance and decrease the power conversion efficiency (PCE).

Plasmonic nanoparticles offer another option to improve the photocurrents.[8−11] The improvement is based on at least two effects, namely, the near field antenna effect[12,13] and the far field scattering effect.[14−16] A plasmonic nanoparticle traps a photon on the basis of localized surface plasmon resonance (LSPR), and generates a strong oscillating electric field (*i.e.*, optical

* Address correspondence to tatsuma@iis.u-tokyo.ac.jp, csegawa@mail.ecc.u-tokyo.ac.jp.

Received for review January 15, 2015 and accepted March 18, 2015.

Published online March 18, 2015
10.1021/acsnano.5b00321

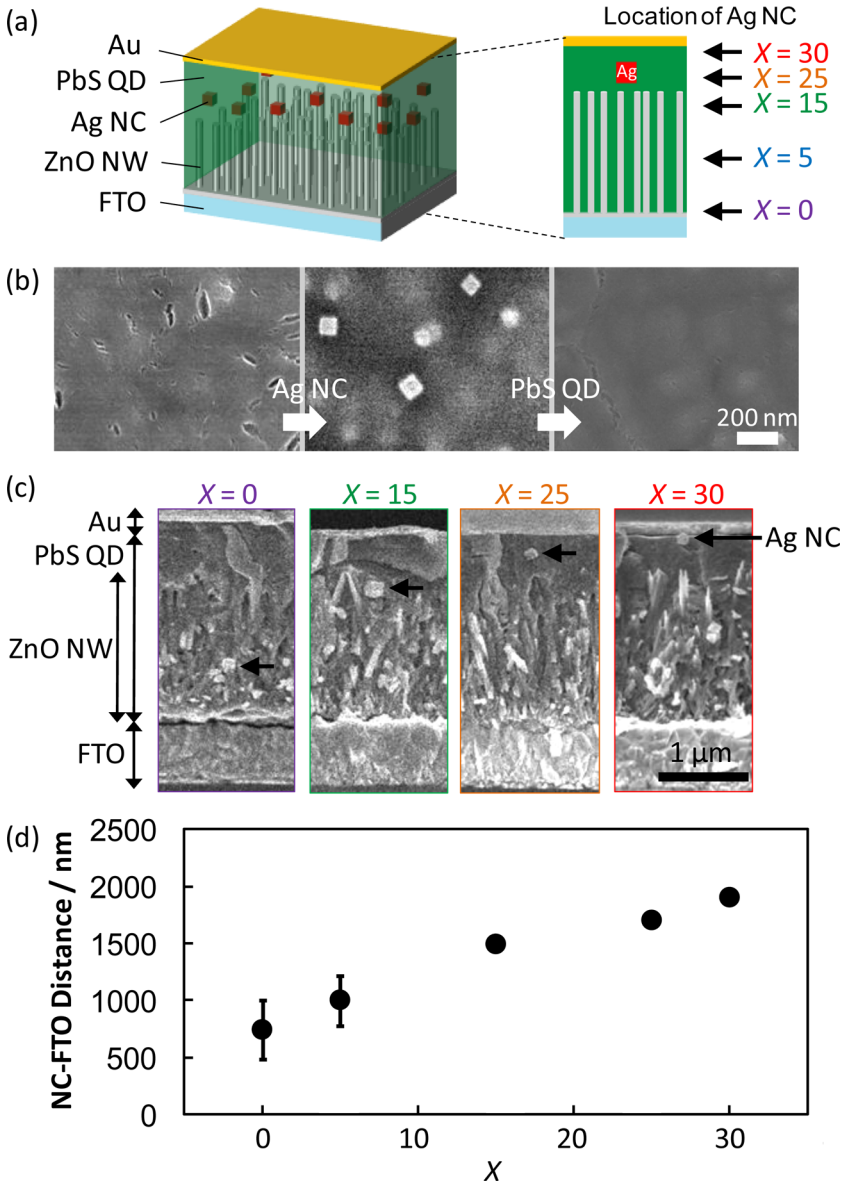

Figure 1. (a) Schematic of a PbS QD/ZnO NW solar cell with embedded Ag NCs. (b, c) Scanning electron micrographs of the cell. (b) Top views before and after casting of Ag NCs and after further coating with a PbS QD layer ($X = 25$, NC coverage = 2.1%). (c) Cross-sectional views for different X values. (d) Relationship between the NC-FTO distance and the X value. See text for definition of X.

near field) that is localized in the vicinity of the nanoparticle. The optical near field excites a dye molecule or semiconductor more efficiently than incident far field light. Photocurrents are thus enhanced by the near field antenna effect. On the other hand, photocurrent enhancement due to far field scattering effect is explained in terms of an increased number of incident photons through a glass window or increased effective light path length in the solar cell by far field scattering light from the plasmonic nanoparticles. To red-shift the LSPR wavelength to the near-infrared region, plasmonic nanorods,[8,17] nanoshells,[8] and nanosphere dimers[18] are used typically. Actually, Sargent *et al.* used plasmonic nanorods and nanoshells for efficiency enhancement of colloidal QD solar cells with a planar junction.[8]

Here we apply plasmonic Ag nanocubes (NCs) to QD bulk-heterojunction solar cells (Figure 1a) for the first time, aiming at enhanced photocurrents and PCE, particularly in the near-infrared region. Plasmonic NCs,[19] which combine advantages of the nanoparticles mentioned above, exhibit LSPR in response to light of any incident and polarization angle and generates a strong optical near field at each edge and each vertex.[20,21] In addition, NCs of relatively large size exhibit strong far field scattering. In the case of colloidal QD solar cells with a planar junction, the position of QDs in those cells has been optimized by means of theoretical simulation.[8] However, effects of the position and amount of Ag NCs in QD heterojunction solar cells have never been studied systematically and

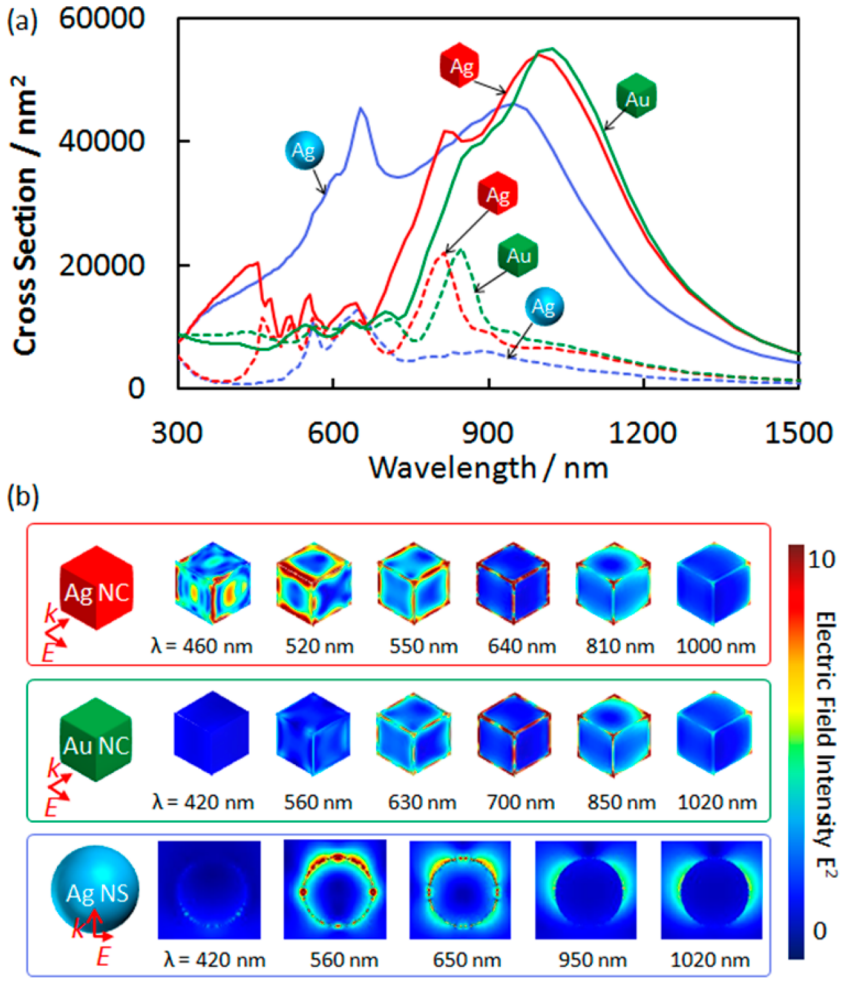

Figure 2. (a) Scattering (solid lines) and absorption (dashed lines) spectra and (b) electric field distributions for Ag and Au NCs (edge length = 80 nm) and a Au NS (diameter = 100 nm) in a PbS QD matrix (refractive index n = 2.6).

experimentally to the best of our knowledge. In the case of QD bulk-heterojunction solar cells, it is difficult to accurately simulate the optical behavior because of the complex structure. In this paper, we carried out systematic studies on efficiency enhancement of PbS QD/ZnO nanowire (NW) solar cells by controlling the position and amount of Ag NCs, and found out optimal conditions. As a result, photocurrents are improved particularly in the near-infrared region and PCE under AM1.5G illumination (100 mW cm^{-2}) is enhanced from 4.5% to 6.0%.

RESULTS AND DISCUSSION

Spectral Simulation of Metal Nanoparticles. As described above, plasmonic nanoparticles enhance photocurrents on the basis of the near-field antenna effect and far field scattering effect. On the other hand, when plasmonic nanoparticles are introduced to highly efficient solar cells, there is a possibility that the efficiency is lowered by nonradiative decay of the nanoparticles. To remove such a negative factor and take advantage of the positive effects, nanoparticles that exhibit strong near fields, strong scattering, and weak absorption should be selected.

We therefore calculated the scattering and absorption spectra as well as electric field distributions for nanoparticles with almost the same volume, Ag and Au NCs (edge length = 80 nm, edge curvature radius = 10 nm) and a Ag nanosphere (NS, diameter = 100 nm), in a PbS QD matrix by a finite-difference time-domain (FDTD) method. In general, when a plasmonic nanoparticle is surrounded by a medium of high refractive index, its resonance is red-shifted and enhanced.[22,23] The refractive index of a PbS QD layer that is prepared by a similar method is reported to be ~2.6 at 1000 nm.[24] Figure 2a shows the calculated spectra. The Ag and Au NCs exhibit strong scattering in a longer wavelength region than the Ag NS. Since their scattering is strong in the wavelength range 700−1200 nm, in which light absorption of the PbS QD is relatively low, the Ag and Au NCs are more suitable for the far field scattering than the Ag NS. In addition, the Ag NC has lower absorption cross-section than the Au NC in the range 300−450 nm because of less significant interband transitions. Ag NCs are therefore less likely to block light absorption of PbS QDs in this wavelength range.

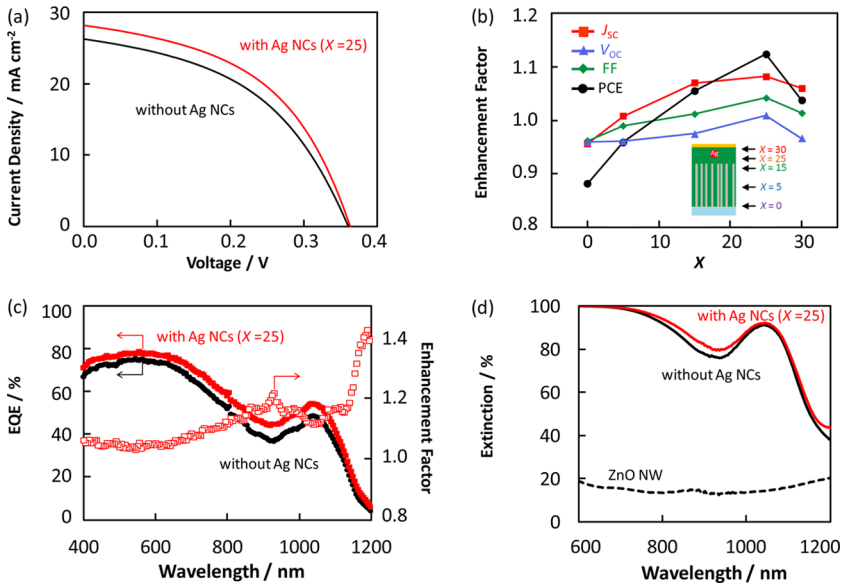

Figure 3. (a) $J-V$ characteristics of the PbS QD/ZnO NW solar cells without and with Ag NCs (X = 25). (b) Enhancement factors of J_{SC}, V_{OC}, FF, and PCE for the cells with different Ag NC positions. (c) EQE action spectra and (d) extinction spectra of the cells without and with Ag NCs (X = 25). Action spectrum of the EQE enhancement factor is also plotted in (c). Ag NC coverage is 2.1% for the cells with NCs.

On the other hand, from the viewpoint of the near field antenna effect, localized electric fields generated around the particles are of importance. Thus, we calculated the electric field distributions at the scattering peak wavelengths and some other wavelengths of each particle (Figure 2b). It is reported that a Ag NC has at least six plasmon modes.[20] In the PbS QD matrix, the present Ag NC exhibits seven scattering peaks in the range 300−1500 nm. The electric field distribution is different for different resonance modes. However, electric fields are localized mainly on the vertices and edges of the NC in general. The Ag NC exhibits strong electric fields in the broader wavelength range than does the Au NC. On the basis of these results, we employed Ag NCs for efficiency enhancement experiments of the PbS QD/ZnO NW bulk-heterojunction solar cells.

Optimization of NC Position. When plasmonic nanoparticles are introduced into solar cells, their position is important. The near field antenna effect is valid only in the range 100 nm or less from the particle surface.[12,13,25,26] On the other hand, nanoparticles may block the light incidence to the QDs behind. It is difficult to accurately calculate all those effects as well as far field scattering for the present cells with complex structures, in particular ZnO NWs, which are not completely straight and vertical. Therefore, we experimentally optimized the position of Ag NCs in the PbS QD/ZnO NW cells in terms of PCE and other cell performances.

An FTO-coated glass plate (FTO = F-doped SnO_2) was covered with a ZnO seed layer (thickness = 100 nm) and ZnO NWs were grown (length = 1.5 μm). PbS QDs (the first exciton absorption peak = 1030 nm, estimated diameter = 3.4 nm) were spin-coated 35 times onto the ZnO NWs. The Ag NCs were introduced by casting after the Xth coating, followed by further 30 X times coating of QDs (Figure 1a, b). Cross sections of the prepared cells were observed by scanning electron microscopy (Figure 1c), and the average distance from the FTO surface was plotted as a function of the X value in Figure 1d. The variation of the position is large for X = 0 and 5, because the NCs tend to be trapped at the NW surface. In contrast, for X = 15, 25, and 30, the variation is small. Ag NCs almost maintained the cubic shape in the PbS QD layer.

We obtained current−voltage ($J-V$) curves of the plamonic PbS QD/ZnO NW cells under AM1.5G (100 mW cm^{-2}) illumination (Figure 3a), and evaluated short-circuit current density (J_{SC}), open-circuit voltage (V_{OC}), fill factor (FF), and PCE for different X values. Figure 3b illustrates the enhancement factors for those values (*i.e.*, ratio of the value for the cell with NCs to that without NCs) as functions of the X value. The highest enhancement is reached at X = 25 in all the cases. The cell performances for X = 0 were the lowest among the cells examined including the cell without the Ag NCs.

The EQE values, which are evaluated from J_{SC} values and the numbers of incident photons, for the cell with NCs (X = 25) and that without NCs and the ratio between them (*i.e.*, enhancement factor for EQE) are plotted against the irradiation wavelength in Figure 3c. Corresponding spectra of percent of extinction (=100 − % transmittance) for those two cells are also shown in Figure 3d. The enhancement spectrum is rather featureless in comparison to the simulated spectra because the nanocubes are diverse in the size and orientation. The enhancement of EQE is large in

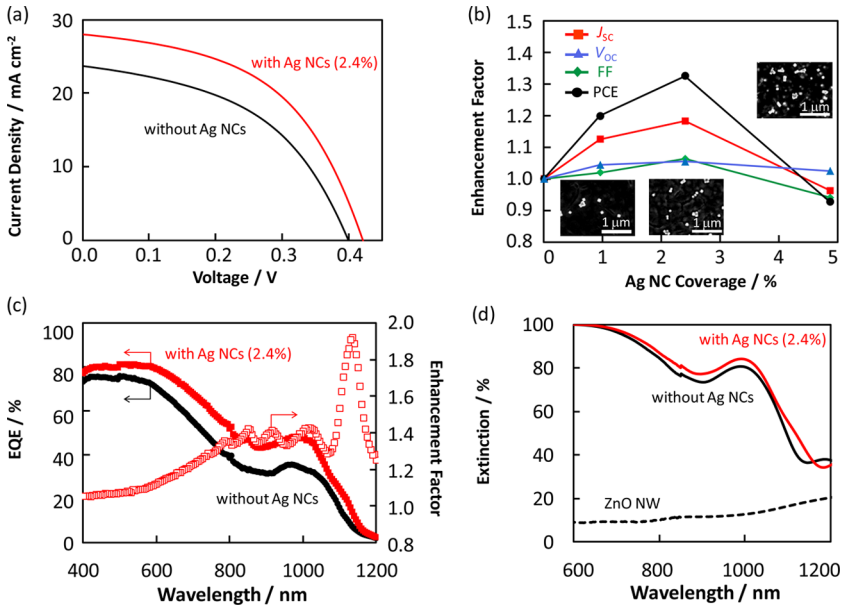

Figure 4. (a) $J-V$ characteristics of the PbS QD/ZnO NW solar cells without and with Ag NCs (coverage =2.4%). (b) Enhancement factors of J_{SC}, V_{OC}, FF, and PCE for the cells with different Ag NC coverage. (c) EQE action spectra and (d) extinction spectra of the cells without and with Ag NCs (2.4%). Action spectrum of the EQE enhancement factor is also plotted in (c). Ag NC position X = 20 for the cells with NCs.

the wavelength range where the extinction of the PbS QD layer is relatively low (700−1200 nm). NCs for $X = 25$ should therefore assist PbS QDs in effective absorption of photons. The enhancement can be explained in terms of the near field antenna effect and the far field scattering effect, as described above. Although it is difficult to evaluate their contributions, that of the scattering effect should be significant because the NCs have several times larger scattering cross section than the absorption cross section at 900−1200 nm (Figure 2a). However, if the NCs are close to FTO (*i.e.*, X = 0), they reduce photocurrents by shielding the PbS QDs behind or insufficient infiltration of PbS QDs. The photocurrent enhancement is also reduced when the NCs are too close to the Au counter electrode (*i.e.*, $X = 30$). This can be explained as follows. The QDs around the NCs are too far from the ZnO NWs to make a significant contribution to photocurrents because of hole−electron recombination. Therefore, the NCs cannot contribute to the photocurrent enhancement significantly in terms of the near field antenna effect. Contribution of the Ag NCs in terms of the far field scattering effect may also be reduced because of weakened light scattered from the NCs to the PbS/ZnO interfacial region.

The V_{OC} and FF values are greatly affected by recombination of electron−hole pairs in the PbS QD layer. When the X value is small, the V_{OC} and FF values are lower than those for the cell without NCs, likely because electrons injected from QDs to NWs go back to the QDs through some Ag NCs that are in contact with the NWs. The back electron transfer lowers the Fermi level of the ZnO NWs and reduces V_{OC}. This leakage path also decreases the parallel resistance and the FF value. Actually, the parallel resistance evaluated on the basis of the $J-V$ curves decreased from 2.37 × 10^3 to 1.85 × 10^3 Ω·cm^2 after introducing the Ag NCs ($X = 0$). Thus, we conclude that there is the optimum position of Ag NCs in terms of the cell performance. As a result of the introduction of plasmonic Ag NCs to the optimized position, the PCE of the PbS QD/ZnO NW solar cell was increased from 4.37% to 4.91% by 1.12 times.

Optimization of NC Amount. Next we optimized the amount of Ag NCs in the cell. In the last section, we optimized the NC location, and found that the enhancement of efficiency was chiefly due to improvement in J_{SC}. Therefore, in this section, we adopted the cell arrangement for higher V_{OC} and lower J_{SC} before introduction of Ag NCs. The cell has shorter ZnO NWs (1.2 μm) and a thinner PbS QD layer. The total number of QD (first exciton absorption peak = 980 nm, estimated diameter = 3.2 nm) coating cycles was 30, and we located the Ag NCs at X = 20. We controlled the amount of NCs by changing the casting amount (Figure 4b, inset). We calculated ratio of the total cross-sectional area of the NCs to the casting area as the index of the NC amount. The NC coverage (*i.e.*, ratio of the total cross-sectional area of NCs to the cell area) of the cells used for Figure 3 was around 2.1%.

Figure 4b shows the dependencies of the enhancement factors for J_{SC}, V_{OC}, FF, and PCE on the amount of Ag NCs embedded in the PbS QD/ZnO NW cells. The $J-V$ curves for the cell showing the best performances and the cell without NCs are shown in Figure 4a. As the amount of Ag NCs increases, all of the enhancement factors increase, and the maximum values are reached

at 2.4% coverage, followed by a drop in the enhancement factors. It is obvious that J_{SC} mainly contributes to the enhancement of the PCE.

The EQE action spectra of the cell with Ag NCs (2.4%) and that without NCs as well as the action spectrum of EQE enhancement factor are shown in Figure 4c. Again, the photocurrent enhancement is significant in the range 700−1200 nm. Interestingly, the average EQE enhancement at 800−1100 nm (1.37, Figure 4c) looks greater than the extinction enhancement (Figure 4d). Although it is difficult to exclude the contribution of reflection and scattering at the ZnO surface completely, the enhancement of the percent of extinction of the QD layer should be less than 1.2. In addition, the photocurrents are enhanced even in the visible region, in which the light absorption of PbS QDs is almost saturated. These results suggest that the internal quantum efficiency (IQE) is enhanced by Ag NCs, for instance owing to improved charge separation efficiency in the PbS QD layer. Enhancement of exciton dissociation by plasmonic nanoparticles has recently been reported for HgTe quantum dot photodiodes[27] and different types of solar cells.[11,28−32] This may also be the case for the present system. In either event, the optimization of the NC amount resulted in the improvement of the PCE from 4.45% (without Ag NCs) to 6.03% by 1.36 times.

The enhancement in the charge separation efficiency can be responsible for the slight improvement in the V_{OC} and FF as well. The decreased cell performance at 4.9% coverage in Figure 4b is attributed to excess Ag NCs, which suppress the charge separation efficiency because of electron−hole recombination at NCs and energy transfer[25] from excited QDs to NCs. The recombination effect might be more significant for aggregated NCs.

It is noteworthy that a peak at ∼1100 nm and some small features are seen in the extinction enhancement spectrum in Figure 4d and are reflected by the photocurrent enhancement spectrum in Figure 4c. These features may be explained in terms of electric field-induced[33] or electrochemically induced[34] modulation of the QD spectrum. It is known for the former that the linear combination of the first and second derivative of extinction ($d\,\text{extinction}/d\lambda$ and $d^2\text{extinction}/d\lambda^2$, reapectively) fits well to extinction changes.[33] In the present case, the second derivative of the extinction spectrum in Figure 4d (black curve) gives local maxima at 769, 837, 900, and 1113 nm, in good accordance with the peaks in the extinction enhancement (dashed red curve). The electrochemically induced modulation, if any, may be related to plasmon-induced charge separation at the interface between a plasmonic nanoparticle and a semiconductor.[35] In either event, the strong plasmonic near field may also be responsible for the peak and small features.

CONCLUSIONS

The plasmonic Ag NC (edge length = 80 nm) shows strong far field scattering in the wavelength region where PbS QDs exhibit weak absorption and the NC generates intense optical near field in the visible and near-infrared regions. Photocurrents of the PbS QD/ZnO NW bulk-heterojunction solar cells are enhanced by introduction of the Ag NCs particularly in the range 700−1200 nm. NCs make effective use of light when those are located relatively far from the FTO electrode. The photocurrent enhancement is ascribed to plasmonic enhancement of light absorption and possible facilitation of exciton dissociation. Introduction of excess NCs, however, results in enhanced charge recombination and suppressed photocurrents. As a result of the optimization of the position and amount of Ag NCs, the PCE of PbS QD/ZnO NW bulk-heterojunction solar cells is improved to 6.03% by 1.36 times.

METHODS

Syntheses. PbS QDs were synthesized according to the method of Sargent *et al.*[36] with minor modifications. Octadecene (ODE) was degassed at 85 °C for 2 h, and 3 mL of ODE was mixed with 0.45 g of PbO and 1.8 mL of oleic acid and heated at 95 °C under vacuum for 2 h. The solution thus obtained (4.5 mL) was mixed with 15 mL of ODE and heated at 125 °C under Ar, followed by addition of 0.18 mL bis(trimethylsilyl)sulfide in 10 mL of ODE. The solution was cooled to 35 °C over ∼1 h. The resultant solution was mixed with 10 mL of toluene and 40 mL of acetone and centrifuged to isolate the PbS QDs. This washing step was repeated several times, and the PbS QDs were redispersed in octane.

Ag NCs (average edge length = 79.2 ± 5.6 nm, n = 90) were synthesized by the method reported by Xia *et al.*[37] with slight modifications.[38] Ethylene glycol (EG, 5 mL) was stirred at 140−145 °C in a 20 mL capped vial for 1 h, followed by addition of 3 mM HCl in 1 mL EG. After stirring for 10 min, 94 mM $AgNO_3$ in 3 mL of EG and 147 mM poly(vinylpyrrolidone) (monomer unit, M_r ∼ 55 000) in 3 mL of EG were added simultaneously to the stirred solution at 45 mL h^{-1}, followed by stirring at 140−145 °C for ∼2 h. The NCs were precipitated by addition of excess acetone, separated by centrifugation, and resuspended in ethanol.

A 100 nm thick ZnO seed layer was formed on a FTO-coated glass plate (sheet resistance = 10 Ω/sq) by a spin-coating method. ZnO NWs (1.2 or 1.5 μm long) were vertically grown on the seed layer by hydrothermal synthesis method.[7]

Device Fabrication. The PbS QDs were infiltrated into the ZnO NW layer from a PbS QD octane solution (50 mg mL^{-1}) *via* a layer-by-layer spin-coating method. Each PbS QD layer was treated with a cetyltrimethylammonium bromide (CTAB) methanol solution (10 mg mL^{-1}) to replace insulating oleic acid chain ligands with bromide anions.[36] The substrate was then rinsed with methanol to remove excess CTAB and oleic acid. After the coating process was repeated X (= 0, 5, 15, 25, 30) times, 0.203 g mL^{-1} Ag NC dispersion was cast on the QD layer and heated at 60 °C to evaporate ethanol. Then the QD coating process was repeated 35 X or 30 X cycles. Finally, a Au back contact (100 nm thick) was deposited on top of the PbS QD layer

by thermal evaporation. In order to minimize possible influence of differences in the size and so forth of NWs and QDs, we used those of the same lot in each optimization of the NC position or amount.

Device Characterization. We obtained EQE action spectra using a 250 mm monochromator equipped with a 150 W Xe lamp (photon flux = 1.66 μmol m^{-2}). The J–V characteristics were measured by scanning V_{OC} at 55 mV s^{-1} with a source meter (2611A Keithley) under AM1.5G irradiation (100 mW cm^{-2}) from a solar simulator (Bunkoukeiki, CEP-2000MLQ). All the measurements were performed on the solar cells without encapsulation in air using a metal mask with a 2.5 mm diameter aperture.

FDTD Simulations. We simulated scattering and absorption spectra and the localized electric fields around a metal nanoparticle in a PbS QD matrix (refractive index = 2.6[24]) by a FDTD method (Lumerical Solutions). The simulation domain (1000 × 1000 × 1000 nm^3) consisted of 100 nm cubic cells, and the central region (150 × 150 × 150 nm^3) was further meshed with a three-dimensional grid of 1 nm spacing. The dielectric functions of Au and Ag were extracted from the data of Johnson and Christy[39] and Lynch and Hunter,[40] respectively.

Conflict of Interest: The authors declare no competing financial interest.

Acknowledgment. This work was supported in part by New Energy and Industrial Technology Development Organization (NEDO), the Japan Science and Technology Agency (JST) thorough its "Funding Program for Core Research for Evolutional Science and Technology (CREST)", and a Grant-in-Aid for Scientific Research No. 25107511. T.K. thanks a JSPS Research Fellowship for Young Scientists.

REFERENCES AND NOTES

1. Kramer, I. J.; Sargent, E. H. The Architecture of Colloidal Quantum Dot Solar Cells: Materials to Devices. *Chem. Rev.* **2014**, *114*, 863–882.
2. Moreels, I.; Lambert, K.; Smeets, D.; De Muynck, D.; Nollet, T.; Martins, J. C.; Vanhaecke, F.; Vantomme, A.; Delerue, C.; Allan, G.; et al. Size-Dependent Optical Properties of Colloidal PbS Quantum Dots. *ACS Nano* **2009**, *3*, 3023–3030.
3. Chuang, C. H.; Brown, P. R.; Bulovic, V.; Bawendi, M. G. Improved Performance and Stability in Quantum Dot Solar Cells Through Band Alignment Engineering. *Nat. Mater.* **2014**, *13*, 796–801.
4. Luther, J. M.; Gao, J. B.; Lloyd, M. T.; Semonin, O. E.; Beard, M. C.; Nozik, A. J. Stability Assessment on a 3% Bilayer PbS/ZnO Quantum Dot Heterojunction Solar Cell. *Adv. Mater.* **2010**, *22*, 3704–3707.
5. Brown, P. R.; Lunt, R. R.; Zhao, N.; Osedach, T. P.; Wanger, D. D.; Chang, L. Y.; Bawendi, M. G.; Bulovic, V. Improved Current Extraction from ZnO/PbS Quantum Dot Heterojunction Photovoltaics Using a MoO_3 Interfacial Layer. *Nano Lett.* **2011**, *11*, 2955–2961.
6. Wang, H.; Kubo, T.; Nakazaki, J.; Kinoshita, T.; Segawa, H. PbS-Quantum-Dot-Based Heterojunction Solar Cells Utilizing ZnO Nanowires for High External Quantum Efficiency in the Near-Infrared Region. *J. Phys. Chem. Lett.* **2013**, *4*, 2455–2460.
7. Wang, H.; Kubo, T.; Nakazaki, J.; Segawa, H. PbS Colloidal Quantum Dot/ZnO-Based Bulk-Heterojunction Solar Cells with High Stability under Continuous Light Soaking. *Phys. Status Solidi RRL* **2014**, *8*, 961–965.
8. Paz-Soldan, D.; Lee, A.; Thon, S. M.; Adachi, M. M.; Dong, H.; Maraghechi, P.; Yuan, M.; Labelle, A. J.; Hoogland, S.; Liu, K.; et al. Jointly Tuned Plasmonic–Excitonic Photovoltaics Using Nanoshells. *Nano Lett.* **2013**, *13*, 1502–1508.
9. Kholmicheva, N.; Moroz, P.; Rijal, U.; Bastola, E.; Uprety, P.; Liyanage, G.; Razgoniaev, A.; Ostrowski, A. D.; Zamkov, M. Plasmonic Nanocrystal Solar Cells Utilizing Strongly Confined Radiation. *ACS Nano* **2014**, *8*, 12549–12559.
10. Wu, J.; Mangham, S. C.; Reddy, V. R.; Manasreh, M. O.; Weaver, B. D. Surface Plasmon Enhanced Intermediate Band Based Quantum Dots Solar Cell. *Sol. Energy Mater. Sol. Cells* **2012**, *102*, 44–49.
11. Wu, J.; Yu, P.; Susha, A. S.; Sablon, K. A.; Chen, H.; Zhou, Z.; Li, H.; Ji, H.; Niu, Z.; Govorov, A. O. Broadband Efficiency Enhancement in Quantum Dot Solar Cells Coupled with Multispiked Plasmonic Nanostars. *Nano Energy* **2015**, 10.1016/j.nanoen.2015.02.012.
12. Standridge, S. D.; Schatz, G. C.; Hupp, J. T. Distance Dependence of Plasmon-Enhanced Photocurrent in Dye-Sensitized Solar Cells. *J. Am. Chem. Soc.* **2009**, *131*, 8407–8409.
13. Kawawaki, T.; Takahashi, Y.; Tatsuma, T. Enhancement of Dye-Sensitized Photocurrents by Gold Nanoparticles: Effects of Dye-Particle Spacing. *Nanoscale* **2011**, *3*, 2865–2867.
14. Stenzel, O.; Stendal, A.; Voigtsberger, K.; von Borczyskowski, C. Enhancement of the Photovoltaic Conversion Efficiency of Copper Phthalocyanine Thin Film Devices by Incorporation of Metal Clusters. *Sol. Energy Mater. Sol. Cells* **1995**, *37*, 337–348.
15. Stuart, H. R.; Hall, D. G. Island Size Effects in Nanoparticle-Enhanced Photodetectors. *Appl. Phys. Lett.* **1998**, *73*, 3815–3817.
16. Catchpole, K. R.; Polman, A. Plasmonic Solar Cells. *Opt. Express* **2008**, *16*, 21793–21800.
17. Chang, S.; Li, Q.; Xiao, X.; Wong, K. Y.; Chen, T. Enhancement of Low Energy Sunlight Harvesting in Dye-Sensitized Solar Cells Using Plasmonic Gold Nanorods. *Energy Environ. Sci.* **2012**, *5*, 9444–9448.
18. Kawawaki, T.; Takahashi, Y.; Tatsuma, T. Enhancement of Dye-Sensitized Photocurrents by Gold Nanoparticles: Effects of Plasmon Coupling. *J. Phys. Chem. C* **2013**, *117*, 5901–5907.
19. Baek, S.-W.; Park, G.; Noh, J.; Cho, C.; Lee, C.-H.; Seo, M.-K.; Song, H.; Lee, J.-Y. Au@Ag Core–Shell Nanocubes for Efficient Plasmonic Light Scattering Effect in Low Bandgap Organic Solar Cells. *ACS Nano* **2014**, *8*, 3302–3312.
20. Zhang, S.; Bao, K.; Halas, N. J.; Xu, H.; Nordlander, P. Substrate-Induced Fano Resonances of a Plasmonic Nanocube: a Route to Increased-Sensitivity Localized Surface Plasmon Resonance Sensors Revealed. *Nano Lett.* **2011**, *11*, 1657–1663.
21. Moreau, A.; Ciraci, C.; Mock, J. J.; Hill, R. T.; Wang, Q.; Wiley, B. J.; Chilkoti, A.; Smith, D. R. Controlled-Reflectance Surfaces with Film-Coupled Colloidal Nanoantennas. *Nature* **2012**, *492*, 86–89.
22. Atwater, H. A.; Polman, A. Plasmonics for Improved Photovoltaic Devices. *Nat. Mater.* **2010**, *9*, 205–213.
23. Beck, F. J.; Polman, A.; Catchpole, K. R. Tunable Light Trapping for Solar Cells Using Localized Surface Plasmons. *J. Appl. Phys.* **2009**, *105*, 114310.
24. Adachi, M. M.; Labelle, A. J.; Thon, S. M.; Lan, X.; Hoogland, S.; Sargent, E. H. Broadband Solar Absorption Enhancement *via* Periodic Nanostructuring of Electrodes. *Sci. Rep.* **2013**, *3*, 2928.
25. Kawawaki, T.; Tatsuma, T. Enhancement of PbS Quantum Dot-Sensitized Photocurrents Using Plasmonic Gold Nanoparticles. *Phys. Chem. Chem. Phys.* **2013**, *15*, 20247–20251.
26. Torimoto, T.; Horibe, H.; Kameyama, T.; Okazaki, K.-i.; Ikeda, S.; Matsumura, M.; Ishikawa, A.; Ishihara, H. Plasmon-Enhanced Photocatalytic Activity of Cadmium Sulfide Nanoparticle Immobilized on Silica-Coated Gold Particles. *J. Phys. Chem. Lett.* **2011**, *2*, 2057–2062.
27. Chen, M.; Shao, L.; Kershaw, S. V.; Yu, H.; Wang, J.; Rogach, A. L.; Zhao, N. Photocurrent Enhancement of HgTe Quantum Dot Photodiodes by Plasmonic Gold Nanorod Structures. *ACS Nano* **2014**, *8*, 8208–8216.
28. Zhang, W.; Saliba, M.; Stranks, S. D.; Sun, Y.; Shi, X.; Wiesner, U.; Snaith, H. J. Enhancement of Perovskite-Based Solar Cells Employing Core-shell Metal Nanoparticles. *Nano Lett.* **2013**, *13*, 4505–4510.
29. Wu, J.-L.; Chen, F.-C.; Hsiao, Y.-S.; Chien, F.-C.; Chen, P.; Kuo, C.-H.; Huang, M. H.; Hsu, C.-S. Surface Plasmonic Effects of Metallic Nanoparticles on the Performance of Polymer Bulk Heterojunction Solar Cells. *ACS Nano* **2011**, *5*, 959–967.

30. Fung, D. D. S.; Qiao, L.; Choy, W. C. H.; Wang, C.; Sha, W. E. I.; Xie, F.; He, S. Optical and Electrical Properties of Efficiency Enhanced Polymer Solar Cells with Au Nanoparticles in a PEDOT−PSS Layer. *J. Mater. Chem.* **2011**, *21*, 16349–16356.
31. Hao, Y.; Song, J.; Yang, F.; Hao, Y.; Sun, Q.; Guo, J.; Cui, Y.; Wang, H.; Zhu, F. Improved Performance of Organic Solar Cells by Incorporating Silica-Coated Silver Nanoparticles in the Buffer Layer. *J. Mater. Chem. C* **2015**, *3*, 1082–1090.
32. Yao, K.; Xin, X.-K.; Chueh, C.-C.; Chen, K.-S.; Xu, Y.-X.; Jen, A. K.-Y. Enhanced Light-Harvesting by Integrating Synergetic Microcavity and Plasmonic Effects for High-Performance ITO-Free Flexible Polymer Solar Cells. *Adv. Funct. Mater.* **2015**, *25*, 567–574.
33. Klem, E. J. D.; Levina, L.; Sargent, E. H. PbS Quantum Dot Electroabsorption Modulation Across the Extended Communications Band 1200−1700 nm. *Appl. Phys. Lett.* **2005**, *87*, 053101.
34. Wehrenberg, B. L.; Guyot-Sionnest, P. Electron and Hole Injection in PbSe Quantum Dot Films. *J. Am. Chem. Soc.* **2003**, *125*, 7806–7807.
35. Tian, Y.; Tatsuma, T. Mechanisms and Applications of Plasmon-Induced Charge Separation at TiO_2 Films Loaded with Gold Nanoparticles. *J. Am. Chem. Soc.* **2005**, *127*, 7632–7637.
36. Tang, J.; Kemp, K. W.; Hoogland, S.; Jeong, K. S.; Liu, H.; Levina, L.; Furukawa, M.; Wang, X.; Debnath, R.; Cha, D.; et al. Colloidal-Quantum-Dot Photovoltaics Using Atomic-ligand Passivation. *Nat. Mater.* **2011**, *10*, 765–771.
37. Im, S. H.; Lee, Y. T.; Wiley, B.; Xia, Y. Large-Scale Synthesis of Silver Nanocubes: the Role of HCl in Promoting Cube Perfection and Monodispersity. *Angew. Chem., Int. Ed.* **2005**, *44*, 2154–2157.
38. Saito, K.; Tatsuma, T. Asymmetric Three-Way Plasmonic Color Routers. *Adv. Opt. Mater.* **2015**, 10.1002/adom.201500111.
39. Johnson, P. B.; Christy, R. W. Optical Constants of the Noble Metals. *Phys. Rev. B* **1972**, *6*, 4370–4379.
40. Lynch, D. W.; Hunter, W. R. In *Handbook of Optical Constants of Solids*; Palik, E. D., Ed.; Academic Press: New York, 1985.